

Ring-Shaped Jets in Gamma-Ray Bursts *

Ming Xu, Yong-Feng Huang and Si-Wei Kong

Department of Astronomy, Nanjing University, Nanjing 210093, China; hyf@nju.edu.cn

Received 2007 October 18; accepted 2008 January 04

Abstract When the axis of a gamma-ray burst (GRB) does not coincide with the spin axis of its source, there may result a ring-shaped jet. Using some refined jet dynamics, we calculate multi-wavelength afterglow light curves for such ring-shaped jets. In the R-band we find an obvious break in the afterglow light curve due to the beaming effect and the break is affected by many parameters, such as the electron energy fraction ξ_e , the magnetic energy fraction ξ_B^2 , the width of ring $\Delta\theta$ and the medium number density n . The overall light curve can be divided into three power-law stages, i.e., an ultra-relativistic stage, an after-break stage and a deep Newtonian stage. For each stage the power-law index is larger in the ring-shaped jet than in the corresponding conical jet.

Key words: gamma rays: bursts — ISM: jets and outflows

1 INTRODUCTION

Since the first discovery in 1973 (Klebesadel et al. 1973), gamma-ray bursts have become a productive research field. Twenty-three years later, Beppo-SAX obtained the first X-ray afterglow of GRB 970228 (Costa et al. 1997), followed by the discovery of optical afterglow (van Paradijs et al. 1997) and radio afterglow (Frail et al. 1997), which proves that GRBs are located at cosmological distances. The relativistic fireball model is expected to explain this violent event, which suggests that internal shocks produce the prompt main burst emission while external shocks produce the afterglow emission (Piran 1999; Su et al. 2006; Zhang 2007). In order to solve the energy crisis of some GRBs, such as GRB 971214 with an extreme isotropic energy of $0.17 M_\odot c^2$ (Kulkarni et al. 1998), GRB 990123 with $1.9 M_\odot c^2$ (Kulkarni et al. 1999), GRB 990510 with $0.16 M_\odot c^2$ (Harrison et al. 1999), the conical jet model was proposed. For a highly collimated jet, the outflow occupies a small fraction ($f \ll 4\pi$) of the total solid angle, this will reduce the energy output in GRB by a factor f^{-1} . There are various kinds of jets, such as a uniform jet (UJ) (Rhoads 1997) where the energy per solid angle and initial Lorentz factor are uniform within the jet, a universal structured jet (USJ) (Mészáros et al. 1998; Dai & Gou 2001; Zhang & Mészáros 2002) where the energy per solid angle and the initial Lorentz factor are not uniform, a quasi-universal jet (Zhang et al. 2004) where the energy per solid angle is Gaussian but the initial Lorentz factor is uniform, and a two-component jet (Huang et al. 2004; Wu et al. 2005) with a narrow high Lorentz factor inner jet and an outer jet with low initial Lorentz factor.

Another kind of structured jets is ring-shaped outflows, which may be due to a misalignment of the GRB jet axis and the source spin axis (Huang et al. 2003). Granot (2005) has calculated the afterglow light curves of such uniform ring-shaped jets without lateral expansion, using a simple semi-analytic formalism, and found a small break in the light curve, but their calculations were only for the optical bands and neglected the effect of lateral expansion. A more realistic assumption on lateral expansion is obviously necessary, and multi-band afterglow light curves are also needed for comparison with observations.

* Supported by the National Natural Science Foundation of China.

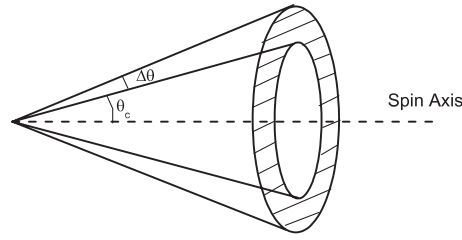


Fig. 1 Sketch of a ring-shaped jet. The dashed line marks the spin axis. The shaded part corresponds to the ring. θ_c is the half opening angle of the inner edge of the ring, $\Delta\theta$ is the width of the ring.

In this paper, we calculate the multi-wavelength afterglow light curves of ring-shaped jets in detail, based on the model developed by Huang et al. (2000a). We include the effects of lateral expansion as well as the equal arrival time surfaces in our calculations. In Section 2, we sketch a simple model of ring-shaped jet. In Section 3 the model is briefly described. In Section 4 we present our detailed numerical results that illustrate the effects of various parameters on the afterglow. Lastly in Section 5 we give our conclusions and a discussion.

2 RING-SHAPED JET

If the GRB jet axis is precessing about the spin axis, the ejecta will be in a spiral shape at first (Fargion & Grossi 2006). The ejecta with different velocities ejected at different time will collide and merge into a uniform ring-shaped jet due to the internal shocks that produce the GRB. Zou & Dai (2006) have investigated the tail emission of such a ring-shaped jet and found an early shallow decay phase and a later re-brightening of the X-ray emission.

A sketch of the ring-shaped jet is shown in Figure 1, where the dashed line is the central axis of the source, the angle of the inner edge of the ring is denoted as θ_c , and the width of the ring is $\Delta\theta$. In view of lateral expansion for a ring-shaped jet, both the inner and the outer edges may expand outward. After a period of time, the inner edge will converge on the central axis and the ring-shaped jet will become eventually a conical jet. The line of sight may be in the center hollow cone or on the ring or even outside of the jet.

3 MODEL

We modify the model developed by Huang et al. (2000a), so as to be applicable to the ring-shaped jet. These models are appropriate for both radiative and adiabatic blastwaves, and for both the ultra-relativistic and non-relativistic stages (Huang et al. 1999).

3.1 Dynamics

The overall dynamics of GRB afterglow has been described by Huang et al. (Huang et al. 1999, 2000a; Huang & Cheng 2003). The model is characterized mainly by the following equation:

$$\frac{d\gamma}{dm} = -\frac{\gamma^2 - 1}{M_{ej} + \epsilon m + 2(1 - \epsilon)\gamma m}, \quad (1)$$

where γ is the bulk Lorentz factor of the shocked medium, m the swept-up mass, M_{ej} the initial ejecta mass, and ϵ the radiative efficiency. The GRB ejecta evolve from the ultra-relativistic stage to the non-relativistic stage. Under realistic conditions, the blastwave becomes adiabatic two or three hours after the main burst (Dai et al. 1999). So we take $\epsilon \equiv 0$ for simplicity.

For the ring-shaped jet, both the inner and outer edge may expand outward. It will become a conical jet when the inner edge converges to the spin axis and only the outer edge will continue with lateral expansion from then on. We suppose that the speed of the lateral expansion is the comoving sound speed c_s given by

$$c_s^2 = \hat{\gamma}(\hat{\gamma} - 1)(\gamma - 1) \frac{1}{1 + \hat{\gamma}(\gamma - 1)} c^2, \quad (2)$$

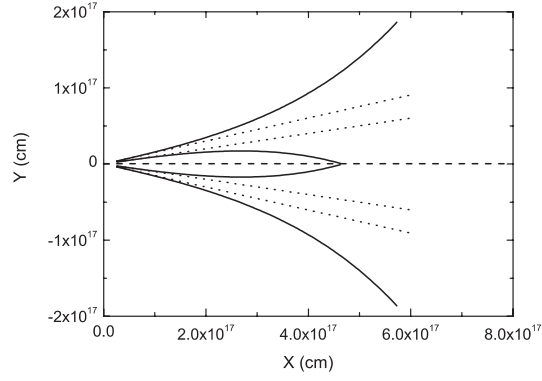


Fig. 2 Schematic illustration of the evolution of the ring-shaped jet on the $X - Y$ plane. X -axis is the spin axis of the jet and the lateral expansion is approximately in Y direction. Solid lines correspond to a “standard” ring-shaped jet with lateral expansion, dotted lines to a jet without lateral expansion. The dashed line marks the center of the ring.

where $\hat{\gamma} \approx (4\gamma + 1)/(3\gamma)$ is the adiabatic index (Dai et al. 1999).

3.2 Radiation

According to the fireball model, afterglows result from the external shocks. Electrons are accelerated by the strong blastwave and produce synchrotron emission, the dominant radiation mechanism. We neglect the inverse Compton scattering here although it may also be important sometimes (Wei & Lu 2000).

For the synchrotron radiation resulting from the shocked-accelerated electrons, we assume the electron energy is distributed in a power-law of index p , the electron energy fraction is ξ_e , and the magnetic energy fraction is ξ_B^2 . We take into account the cooling effect of electrons by using a refined distribution function proposed by Dai et al. (1999). Under these assumptions, the X-ray and optical afterglows can be conveniently calculated, but to calculate the radio afterglow, synchrotron self absorption (SSA) must be considered. We incorporate this effect by using the analytical expressions derived by Wu et al. (2003, 2004).

In view of the effect of equal arrival time surface, the photons received by the observer at any particular time t come from a distorted ellipsoid (Huang et al. 2007). The total observed flux density should be obtained by integrating over the equal arrival time surface determined by

$$\int \frac{1 - \beta \cos \Theta}{\beta c} dR \equiv t, \quad (3)$$

within the jet boundaries (Huang et al. 2000a), where $\beta = \sqrt{\gamma^2 - 1}/\gamma$, Θ is the angle between the velocity of emitting material and the line of sight.

4 NUMERICAL RESULTS

We followed the overall dynamical evolution of ring-shaped jets (from ultra-relativistic to non-relativistic stage) in their X-ray, optical and radio afterglow light curves. We compare the difference between ring-shaped jets and conical jets. The effects of various key parameters on the light curves are also investigated. For convenience, we first define the following initial values as a set of “standard” parameters: initial energy per solid angle $E_0 = 10^{52}/4\pi$ erg, the initial Lorentz factor $\gamma_0 = 300$, the ISM number density $n = 1 \text{ cm}^{-3}$, the index of the power-law energy distribution of electrons $p = 2.5$, the luminosity distance $D_L = 10^6$ kpc, $\xi_B^2 = 0.001$, $\xi_e = 0.1$, $\theta_c = 0.1$, $\Delta\theta = 0.05$ and $\theta_{\text{obs}} = 0.125$, where the observing angle θ_{obs} is defined as the angle between the line of sight and the central axis. For simplicity, we assume that the expansion is completely adiabatic all the time (i.e. $\epsilon \equiv 0$).

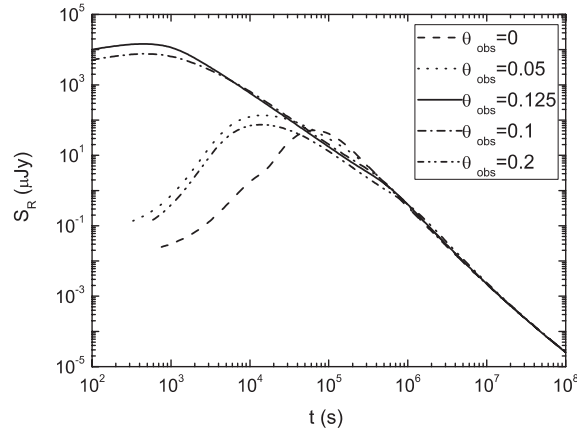


Fig. 3 Effect of the parameter θ_{obs} on the optical light curve. The solid line corresponds to a ring-shaped jet with the “standard” parameters. Other lines are drawn with only θ_{obs} altered.

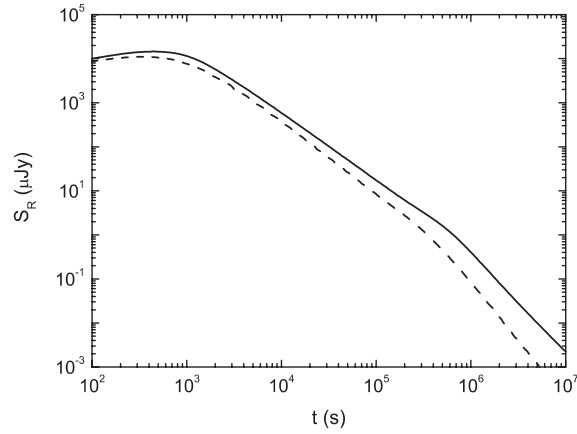


Fig. 4 Optical light curves under the “standard” parameters of a ring-shaped jet without lateral expansion (solid line) and of one with lateral expansion (dashed line).

Figure 2 illustrates schematically the evolution of ring-shaped jets in the $X - Y$ plane, where the X -axis is just the central axis of the jet. The lateral expansion takes place at both the inner and outer edges in the Y direction. The ring-shaped jet become conical when the inner edge converges at the central axis.

Figure 3 shows the effect of altering just the parameter θ_{obs} on the optical afterglow light curves of the ring-shaped jet without lateral expansion, using the model from Section 2. For the viewing angles within the jet (i.e., $\theta_c \leq \theta_{\text{obs}} \leq \theta_c + \Delta\theta$), the light curves are almost unaffected by θ_{obs} . However, the observed fluxes decrease sharply when observed out of the ring, either in the inner hollow cone or outside the jet. It is clear that the more the line of sight deviates from the ring, the more the flux decreases. All the light curves become the same at the later time when the relativistic beaming effect becomes negligible. There is a very small, or even imperceptible, steepening epoch when both edges of the ring become visible (i.e., $\gamma\Delta\theta \sim 1$), which was also shown in Granot (2005). However, we can see an obvious steepening epoch at time T_j , when all of the jet becomes visible (i.e., $\gamma(2\theta_c + 3/2\Delta\theta) \sim 1$) — the expected edge effect.

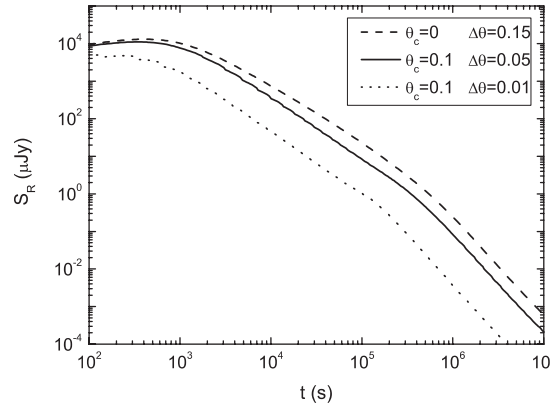


Fig. 5 Effect of the parameter $\Delta\theta$ on the optical light curve for a ring-shaped jet with lateral expansion. The solid line is drawn with the “standard” parameters. The dotted line is drawn with only $\Delta\theta$ altered. The dashed line is for a uniform jet, also viewed at $\theta_{\text{obs}} = 0.125$ ($\theta_c = 0$, $\Delta\theta = 0.15$) and is included for comparison.

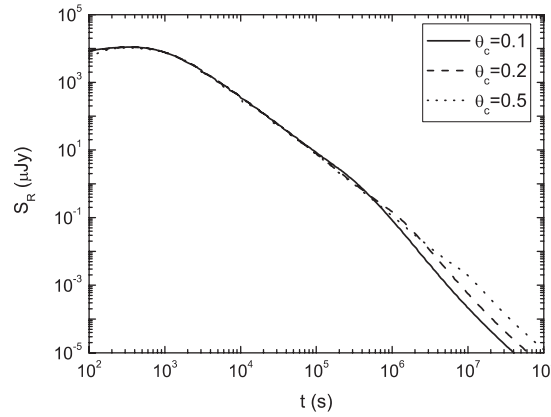


Fig. 6 Effect of the parameter θ_c on the optical light curve for a ring-shaped jet with lateral expansion. The solid line corresponds to a jet drawn with the “standard” parameters. Other lines are drawn with only θ_c altered.

As is shown in Figure 4, after considering a lateral expansion of the ring-shaped jet, the optical afterglow light curve decreases obviously especially for the time after T_j . This is due to the more and more rapid expansion at this stage. So the lateral expansion tends to make the light curve to steepen more obviously and the break to emerge earlier.

In Figure 5, we show the optical afterglow light curves for a line of sight on the ring ($\theta_{\text{obs}} = 0.125$) with lateral expansion, for different ring widths ($\Delta\theta$). It is still hard to see the steepening at the time when $\gamma\Delta\theta \sim 1$, while at $\gamma(2\theta_c + 3/2\Delta\theta) \sim 1$ we can see an obvious break. For comparison, a uniform conical jet viewed at the same viewing angle is shown. With the increase of the value of $\Delta\theta/\theta_c$, we note that the light curves of ring-shaped jet are close to the conical jet. We notice that with the same value of $\theta_c + \Delta\theta$ the observed flux of a ring-shaped jet is smaller than a conical jet, especially at time $t \sim 10^3 - 10^6$ s. This is due to their different shape.

Figure 6 illustrates the effect of the parameter θ_c on the optical afterglow light curve for a ring-shaped jet with lateral expansion. At early time ($t \sim 10^{2.5} - 10^6$ s) the light curves are almost the same for the same width of ring ($\Delta\theta = 0.05$). The most notable difference is the break time T_j : the bigger the inner hollow cone, the later the break time. This is consistent with the relation $\gamma(2\theta_c + 3/2\Delta\theta) \sim 1$, and is due to the edge effect.

Figure 7 illustrates the effect of the parameter ξ_e on the optical afterglow light curve for a ring-shaped jet with lateral expansion. We can see some similar results as did Huang et al. (2000b). For a small ξ_e , an obvious break appears in the light curve, while when ξ_e is large, the break becomes blurred or even disappears. The time that the light curve peaks scales as (Wijers & Galama 1999; Böttcher & Dermer 2000; Chevalier & Li 2000)

$$t_m \propto \left(\frac{p-2}{p-1}\right)^{4/3} \xi_e^{4/3} (\xi_B^2)^{1/3}. \quad (4)$$

From Figure 7 we can see that as ξ_e increases, t_m becomes larger and larger, — this is consistent with Equation (4).

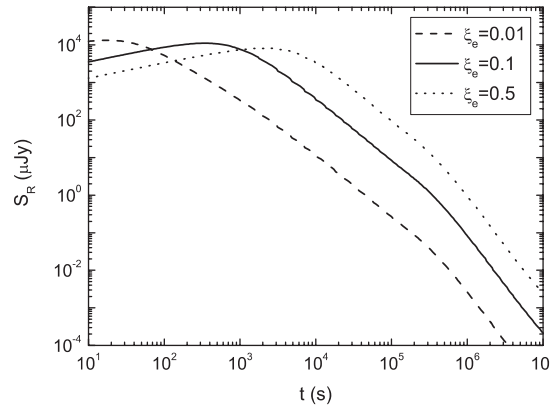


Fig. 7 Effect of the parameter ξ_e on the optical light curve for a ring-shaped jet with lateral expansion. The solid line corresponds to a jet with “standard” parameters. Other lines are drawn with only ξ_e altered.

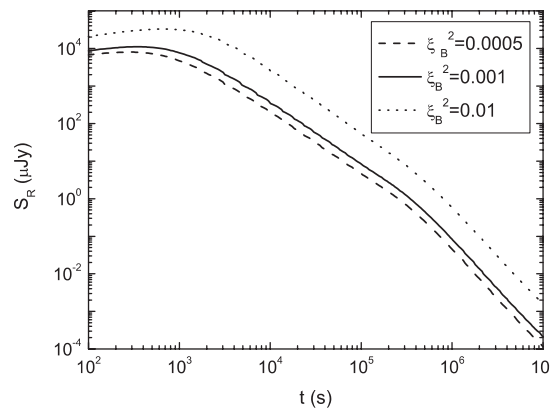


Fig. 8 Effect of the parameter ξ_B^2 on the optical light curve for a ring-shaped jet with lateral expansion. The solid line corresponds to a jet with the “standard” parameters. Other lines are drawn with only ξ_B^2 altered.

Figure 8 illustrates the effect of the parameter ξ_B^2 on the optical afterglow light curve for a ring-shaped jet with lateral expansion. We see an effect similar to the parameter ξ_e : for a small value of ξ_B^2 , there is an obvious break, but for a large value, the break becomes blurred or even disappears. We can also see that with the increase of ξ_B^2 , t_m becomes larger and larger, in agreement with Equation (4).

Figure 9 illustrates the effect of the ISM number density n on the optical afterglow light curve for a ring-shaped jet with lateral expansion. We can see t_m is not related to n under the ultra-relativistic phase, and the peak flux density is consistent with the relation, $S_{R,m} \propto n^{1/2}$ (Wijers & Galama 1999; Böttcher & Dermer 2000). Figure 9 also shows that n affects the steepening of the light curve: with the increase of n , the speed of deceleration becomes faster, so that the light curve break comes earlier.

Figure 10 illustrates the effect of the parameter p on the optical afterglow light curve for a ring-shaped jet with lateral expansion. We can also see that with increasing p , t_m becomes larger, which is consistent with Equation (4), but the most notable difference among the lines is the diversity of the slopes.

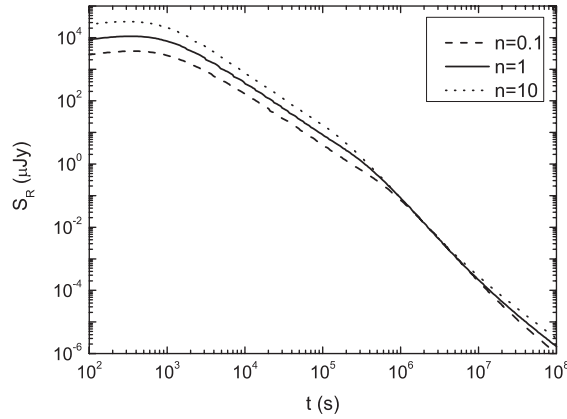


Fig. 9 Effect of the parameter n on the optical light curve for a ring-shaped jet with lateral expansion. The solid line corresponds to a jet with the “standard” parameters. Other lines are drawn with only n altered.

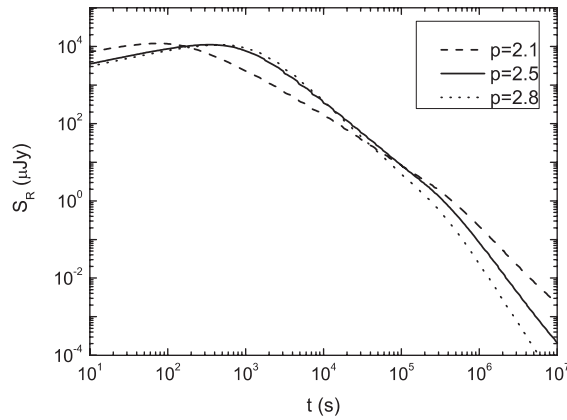


Fig. 10 Effect of the parameter p on the optical light curve for a ring-shaped jet with lateral expansion. The solid line corresponds to a jet with the “standard” parameters. Other lines are drawn with only p altered.

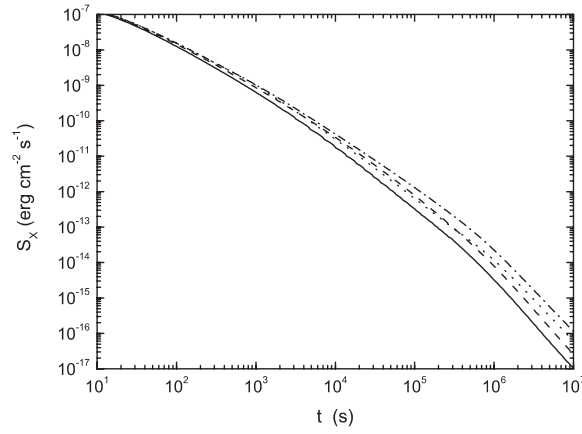


Fig. 11 X-ray afterglow light curves of ring-shaped jets with the “standard” parameters. The solid line corresponds to a ring-shaped jet with lateral expansion and the dotted line, to one without lateral expansion. The X-ray light curves of a conical jet with (dashed line) and without (dash-dotted line) lateral expansion, viewed at $\theta_{\text{obs}} = 0.125$ ($\theta_c = 0$, $\Delta\theta = 0.15$) are also included for comparison.

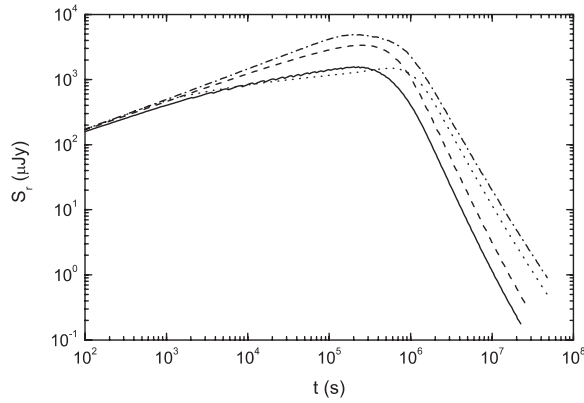


Fig. 12 Radio afterglow light curves of ring-shaped jets with the “standard” parameters. The solid line corresponds to a ring-shaped jet with lateral expansion and the dotted line, to one without lateral expansion. The radio light curves of a conical jet with (dashed line) and without (dash-dotted line) lateral expansion, viewed at $\theta_{\text{obs}} = 0.125$ ($\theta_c = 0$, $\Delta\theta = 0.15$) are also included for comparison.

very different from that of an isotropic fireball and slightly different from conical jet. The time index α varies from $(9p - 6.3)/10$ before T_j to $(11p - 9.1)/7$ after T_j . The increment $\Delta\alpha$ strongly depends on p : $\Delta\alpha = 2(p - 1)/3$.

According to the above figures, the overall optical afterglow light curve can be divided into three power-law stages, with the time index α varying from ~ 1.6 to > 2.5 at T_j fore-and-aft, and with $\alpha \sim 1.7$ in the deep Newtonian phase (which is larger than for a conical jet). The flattening stage is like a spherical shell as the edge effect ceases to exit (Livio & Waxman 2000). This tendency was also shown in the numerical simulation by Huang & Cheng (2003).

Multi-wavelength afterglow light curves are necessary for comparison with the observations. Figure 11 compares the X-ray (0.3–10 keV) afterglow light curves of ring-shaped jets and conical jets. We can see that lateral expansion tends to reduce the brightness, and also to lead to a more rapid decay. The X-ray flux of a ring-shaped jet is smaller than that of a conical jet with the same value of $\theta_c + \Delta\theta$. It is interesting to note that the jet break is not as obvious in the X-ray light curve as in the optical band.

In the optical bands, the emission is usually dominated by contribution from the host galaxy several months later. To better understand the behavior of the afterglow in the deep Newtonian phase, we must resort to radio observations. Radio (8.5 GHz) afterglow light curves of ring-shaped jets and conical jets are shown in Figure 12. We can see some similar features shown in the other bands. The flux is smaller for a ring-shaped jet than for a conical jet with the same $\theta_c + \Delta\theta$. Lateral expansion also tends to make the flux smaller and to lead to a steeper decay.

5 CONCLUSIONS AND DISCUSSION

For GRBs, there may exist ring-shaped jets. For a rotating neutron star, the spin axis and the magnetic axis are likely to point to different directions. As matter is ejected along the magnetic axis, which rotates about the spin axis (Zou & Dai 2006), a ring-shaped jet may be produced. For the model of GRBs associated with neutron star kicks (Huang et al. 2003), when the kick orientation is not parallel to the spin axis of the pulsar, there will also be a ring-shaped jet due to the precessing effect. It is interesting to note that some recent hydrodynamic and MHD simulations have also given some hints on the mechanism of launching a ring-shaped jet (Aloy & Rezzolla 2006; Mizuno et al. 2007).

We have studied the evolution of ring-shaped GRB jets numerically, using the modified model of Huang et al. (2000a) as described in Section 2. The optical afterglow light curves show a very small or even invisible steepening epoch when both edges of the ring become visible (i.e., $\gamma\Delta\theta \sim 1$), but we can see an obvious steepening epoch at time T_j , when all of the jet becomes visible as expected for the edge effect. The optical afterglow light curve of a ring-shaped jet is obviously lower than a conical jet with the same value of $\theta_c + \Delta\theta$. As in the case of a conical jet, the afterglow light curve of a ring-shaped jet is affected by many parameters, such as ξ_e , ξ_B^2 , $\Delta\theta$, and also n . Increasing any of these to some large value will make the break becoming blurred or even disappear. The break in the light curve is due to the jet edge effect and the lateral expansion effect. The parameter θ_c affects T_j : a larger θ_c makes the break to occur later. The parameter p obviously affects the slope: the time index varies as $(9p - 6.3)/10$ before T_j and as $(11p - 9.1)/7$ after T_j and the increment $\Delta\alpha$ strongly depends on p : $\Delta\alpha = 2(p - 1)/3$. These are larger than in the case of a conical jet. In X-ray and radio bands, the afterglow light curves show similar characters as in optical bands.

The X-ray and optical afterglows from a ring-shaped jet are characterized by a very quick decay and an obvious break. After the break, the time index ($\alpha \geq 2.5$) is larger than that of a conical jet and this is quite different from the isotropic fireball. In the deep Newtonian phase, the light curves are relatively flat as expected. Generally, the peak of the light curve appears increasingly later with increasing wavelength.

Acknowledgements We thank Xuefeng Wu for helpful discussion. We also thank the anonymous referee for stimulating suggestions that lead to an overall improvement of this work. This research was supported by the National Natural Science Foundation of China (Grants 10625313 and 10221001).

References

- Aloy M. A., Rezzolla L., 2006, ApJ, 640, L115
 Böttcher M., Dermer C. D., 2000, ApJ, 532, 281
 Chevalier R. A., Li Z. Y., 2000, ApJ, 536, 195
 Costa E., Frontera F., Heise J., Feroci M., in't Zand J. et al., 1997, Nature, 387, 783
 Dai Z. G., Gou L. J., 2001, ApJ, 552, 72
 Dai Z. G., Huang Y. F., Lu T., 1999, ApJ, 520, 634
 Fargion D., Grossi M., 2006, Chin. J. Astron. Astrophys. (ChJAA), 6, 342
 Frail D., Kulkarni S. R., Nicastro L., Feroci M., Taylor G. B., 1997, Nature, 389, 261
 Granot J., 2005, ApJ, 631, 1022
 Harrison F. A. et al., 1999, ApJ, 523, L121
 Huang Y. F., Dai Z. G., Lu T., 1999, MNRAS, 309, 513

- Huang Y. F., Gou L. J., Dai Z. G., Lu T., 2000a, *ApJ*, 543, 90
Huang Y. F., Dai Z. G., Lu T., 2000b, *MNRAS*, 316, 943
Huang Y. F., Dai Z. G., Lu T., Cheng K. S., Wu X. F., 2003, *ApJ*, 594, 919
Huang Y. F., Cheng K. S., 2003, *MNRAS*, 341, 263
Huang Y. F., Lu Y., Wong A. Y. L., Cheng K. S., 2007, *Chin. J. Astron. Astrophys. (ChJAA)*, 7, 397
Huang Y. F., Wu X. F., Dai Z. G., Ma H. T., Lu T., 2004, *ApJ*, 605, 300
Klebesadel R., Strong I., Olson R., 1973, *ApJ*, 182, L85
Kulkarni S. R. et al. 1998, *Nature*, 393, 35
Kulkarni S. R. et al. 1999, *Nature*, 398, 389
Mizuno Y. et al. 2007, *ApJ*, in press, arXiv: 0709.1839
Mészáros P., Rees M. J., Wijers R. A. M. J., 1998, *ApJ*, 499, 301
Livio M., Waxman E., 2000, *ApJ*, 574, 134
Piran T., 1999, *Phys. Rep.*, 314, 575
Rhoads J. E., 1997, *ApJ*, 487, L1
Su C. Y., Qin Y. P., Fan J. H., Han Z. Y., 2006, *Chin. J. Astron. Astrophys. (ChJAA)*, 6, 323
van Paradijs J., Granot P., Galama T., Kouveliotou C., Strom R. et al. 1997, *Nature*, 386, 686
Wei D. M., Lu T., 2000, *A&A*, 360, L13
Wijers R. A. M. J., Galama T. J., 1999, *ApJ*, 523, 177
Wu X. F., Dai Z. G., Huang Y. F., Lu T., 2003, *MNRAS*, 342, 1131
Wu X. F., Dai Z. G., Huang Y. F., Ma H. T., 2004, *Chin. J. Astron. Astrophys. (ChJAA)*, 4, 455
Wu X. F., Dai Z. G., Huang Y. F., Lu T., 2005, *MNRAS*, 357, 1197
Zhang B., 2007, *Chin. J. Astron. Astrophys. (ChJAA)*, 7, 1
Zhang B., Dai X., Lloyd-Ronning N. M., Mészáros P., 2004, *ApJ*, 601, L119
Zhang B., Mészáros P., 2002, *ApJ*, 571, 876
Zou Y. C., Dai Z. G., 2006, *Chin. J. Astron. Astrophys. (ChJAA)*, 6, 551